



Perovskite type nanopowders and thin films obtained by chemical methods

Viktor Fruth¹, Monica Popa¹, Jose Calderon-Moreno¹, Ecaterina Tenea¹, Mihai Anastasescu¹, Petre Osiceanu¹, Elena Anghel¹, Luminita Predoana¹, Barbara Malic², Maria Zaharescu^{1,*}

¹“Ilie Murgulescu” Institute of Physical Chemistry, Romanian Academy, 202 Splaiul Independentei, 060021 Bucharest, Romania

²Jozef Stefan Institute, 39 Jamova, 1001 Ljubljana, Slovenia

Received 21 February 2010; received in revised form 21 August 2010; accepted 3 September 2010

Abstract

The review presents the contribution of the authors, to the preparation of two types of perovskites, namely BiFeO₃ and LaCoO₃, by innovative methods. The studied perovskites were obtained as powders, films and sintered bodies. Their complex structural and morphological characterization is also presented. The obtained results have underlined the important influence of the method of preparation on the properties of the synthesized perovskites.

Keywords: innovative methods, perovskites, thin films, nanopowders

I. Introduction

To obtain oxide materials, conventional ceramic methods based on solid phase reactions at high temperatures are commonly used. In recent years, however, the interest in the synthesis of oxide materials by unconventional methods significantly increased. Some of those methods such as: precipitation/coprecipitation methods, hydrothermal method, the method of decomposition of complex combinations, sol-gel method play an important role.

In the conventional synthesis of ceramics by solid phase reactions, the metal oxides or the corresponding salts, such as for example carbonates, are ground before calcinations to obtain a better homogeneity regarding the composition and the particle size reduction. Due to the fact that the solid phase reactions take place by diffusion, the particle size and metals distribution had a special importance [1]. The repeated stages of calcinations with intermediate grinding are often necessary to improve uniformity and reaction completion. These steps can be additional sources of contamination. High temperatures of calcinations may also affect the stoichi-

ometry by volatilization of the reagents. The problems that are usually associated with solid phase synthesis include the following: a wide particle size distribution, weak sintering capacity, the presence of undesirable intermediate phases. To avoid the disadvantages described above, several new methods were developed, especially techniques in solution, leading to the improvement of the synthesis to obtain pure phases by performing mixing of the reactants at molecular level. In these conditions, the reaction temperatures are significantly lower leading to homogeneous and fine powders [2,3]. Some of the chemical innovative methods are listed below.

The precipitation of metal salts is a classical chemical method which is often used for the synthesis of simple oxides. Adding a chemical reagent that determines the decrease of the solubility limit leads to precipitation. Coprecipitation occurs when different cations in solution precipitate simultaneously [4]. The control of the concentration, temperature, pH, solution homogeneity is essential for the simultaneous precipitation of all cations and to obtain perfectly homogeneous products. The following chemicals may be used as reagents for precipitation: ammonia, ammonium carbonate or ammonium oxalate (which give by decomposition volatile products), urea or hexamethyltetraamina (which

* Corresponding author: tel: +40 21 316 7912
fax: +40 21 312 1147, e-mail: mzaharescu2004@yahoo.com

by step-wise hydrolysis gradually forms ammonium hydroxide in solution). The thermal decomposition of the hydroxides, carbonates or organic salts leads to the corresponding oxide compounds, insoluble in solutions [5].

The principle of *hydrothermal synthesis* is based on a reaction in the aqueous solution or suspension of the precursors at high temperature and pressure. Generally the temperature ranges between 100°C and the critical temperature of water at 374°C. Crystalline powders are obtained and the additional step of calcinations is not required. The particle size and shape can be modified by the reaction temperature, pH, time and concentration of reactants [6].

Thermal decomposition of inorganic complex combination method is another unconventional method of synthesis of the oxide compounds [5]. Among the heteropolynuclear combinations that by relatively low-temperature conversion generate mixed oxides with special properties, the mostly used are those containing carboxylic acid as anionic ligands such as: formic, acetic, oxalic.

“*Pechini*” method [5] allows the synthesis of oxide compounds, with a very good control of the stoichiometry of the reactants and reaction products. Advanced homogeneity and high reproducibility of the reaction mixture exceed the performances of the classical method of synthesis of ceramic compounds expressed in terms of production temperatures and degree of crystallinity. The “*Pechini*” method is also called “the polymeric precursor method” or “the method of mixed liquids”. In principle, the method consists in the formation of a chelate by the reaction of different cations introduced into the system as soluble salts (commonly used are nitrates) with a carboxylic acid (most commonly citric acid). The resulted aqueous solutions containing citric acid and metal salts are then mixed with a desired polyol (most often ethylene glycol) and heated at 80–100°C, resulting in a clear solution. By further heating, between 150–250°C, a condensation reaction occurs involving COOH and OH groups, leading to the formation of a polyester “resin”, in which metallic cations are distributed uniformly in the resin mass.

Among these conventional methods in solution, the sol-gel process based on alkoxides or the sol-gel process in aqueous medium are also included [2,7].

Sol-gel alkoxide route presents a major interest in the field of ceramics. The starting materials, the metallic alkoxide (with general formula $M(OR)_n$), are commercially available for a large variety of metals. As shown by Brinker and Scherer [2], by changing the reaction conditions of the synthesis particles, films, fibers, gels can be obtained. By reactions in the presence of organic compounds, hybrid materials are obtained [8]. The processing of oxide compounds by alkoxide route is based on the hydrolysis and polycondensation of metal-

lic alkoxides $M(OR)_n$.

Sol-gel process in aqueous medium uses inorganic salts and chelating agents of carboxylic acids or polyol type as precursors. The citrate route using citric acid as chelating agent compared to other methods, has the advantage of not only a good mixing of the components at the molecular scale, but also offers the possibility of obtaining films and fibers which have technological importance [9]. Carboxylic precursors are used in the sol-gel route for obtaining oxide materials especially in systems containing transition metals with the role of chelating agents in order to avoid their precipitation. The chemistry of the sol-gel process in aqueous medium, in systems containing transitional metals can be very complicated as several molecular species could be formed depending on the oxidation state of the metal, pH or concentration. In addition, in the case of non-tetravalent cations oxides, hydroxides or oxo-hydroxides are obtained. In the aqueous medium route during the hydrolysis of inorganic salts, new ionic species or precipitates can be formed. Hydrolysis of salts may involve formation of hydrated cations, anions or both types of ions. The hydrolysis of metal cations was first studied by Bjerrum in the early twentieth century [10]. Previous to the studies conducted by Sillen [11], the formation of the polynuclear hydrated compounds was almost ignored. Sillen proposes a mechanism of hydrolysis in which the hydroxyl groups are linked to cations and lead to the formation of condensed species. Now, the iso and heteropoly oxometalate are well known and in the specialized literature there are detailed data about cation hydrolysis [12].

In the present review results concerning the preparation by chemical innovative methods of two types of perovskite, namely $FeBiO_3$ and $LaCoO_3$, are presented. The properties as powders, films and sintered bodies are also discussed.

II. $BiFeO_3$ type perovskites

2.1 $BiFeO_3$ films

The structure and properties of thin films are well known to exhibit a number of deviations from those of bulk ceramics and single crystals. $BiFeO_3$ (BFO) shows unexpectedly small values of the ferroelectric polarization P_s even in a single crystal. Wang *et al.* [13,14] have fabricated an epitaxial monoclinic pseudotetragonal BFO film having $P_s = 90 \text{ C/cm}^2$, almost one order of magnitude higher than that of the bulk BFO by applying a strong compressive stress imposed by the bottom structure, $SrRuO_3/SrTiO_3$. It appears that the crystal structure of $BiFeO_3$ thin films can be affected by the stress and may take different variants depending on the substrate materials, preparing routes and processing conditions. Due to an ever-increasing interest in this promising material as a candidate for multifunctional devices, epitax-

ial and polycrystalline BFO films have been successfully fabricated via various techniques such as pulsed laser deposition (PLD), chemical solution deposition (CSD), magnetron sputtering and others.

Thin films techniques provide routes to structures and phases difficult to obtain by traditional procedures and they also allow properties to be influenced by strain engineering [15]. Studies on the preparation of BiFeO_3 thin films have presented promising potential for improving the ferroelectric polarization, for reducing the leakage current density associated with the low resistivity and high conductivity, and by suppressing the cycloid spin modulation that render an overall zero magnetization.

One practical way to obtain thin ceramic films is the CSD (chemical solution deposition) technique. The general principle involved in the solution deposition of films is to prepare a “homogeneous” solution of the necessary cation species that may later be coated onto a substrate. The fabrication of thin films by this approach involves four basic steps: (i) synthesis of the precursor solution; (ii) deposition by spin-coating or dip-coating, where drying processes usually begin depending on the solvent; (iii) low-temperature heat treatment for drying, pyrolysis of organic species (typically 300–400°C), and formation of an amorphous film; (iv) higher temperature heat treatment for the densification and the crystallization of the coating into the desired oxide phase (600–1100°C). For most solution deposition approaches the final three steps are similar, despite differences in the characteristics of the precursor solution and for electronic devices, spin-coating has been used almost exclusively [16]. Depending on the solution route, different deposition and thermal processing conditions may be employed to control film densification and crystallization for the preparation of materials with optimized

properties [4]. Film shortcomings that could involve changes in solution chemistry include poor thickness uniformity (striations), crack formation, crystallization behaviour and phase purity, and compositional non-uniformities. For the production of BiFeO_3 thin films, the most frequently used CSD approaches may be grouped into different categories: (1) sol–gel [17,18], (2) chelate processes [18], (3) citrate route [19,20], and (4) Pechini process [21–23]. Previously we reported the synthesis of BiFeO_3 powders by combustion and by the polymerizable complex method [24,25].

The citrate solution synthesis is similar to Pechini process, except that ethylene glycol or other polyhydroxy alcohols are not used. By citrate route [26] we have reported the obtaining of BiFeO_3 thin film which has been used to provide homogeneous, single-phase perovskite BiFeO_3 thin films on stainless steel. Stainless steel was chosen as a suitable substrate not only because it is inexpensive but also because being a conductor it can be used as electrode. Samples with a multilayered structure were deposited in order to achieve films with the desired thickness, sometimes impossible to be obtained by only one deposition. On the other hand the thickness of the film cannot be simply obtained by multiplying the thickness of one layer by the numbers of depositions, because each layer from the multilayered structure suffers a different number of thermal treatments and more than that, each new deposited film interacts with the previous one. Fig. 1 shows the XRD pattern of a BiFeO_3 thin film that was deposited from the Bi-Fe precursor solution on steel (A) and on silica glass substrate (B), with heat treatment at 600°C for 1 h.

Single-phase perovskite of BiFeO_3 was obtained already at about 600°C from the decomposition of the complexes. The pattern shows a rhombohedrally distorted perovskite structure. The XRD data showed also

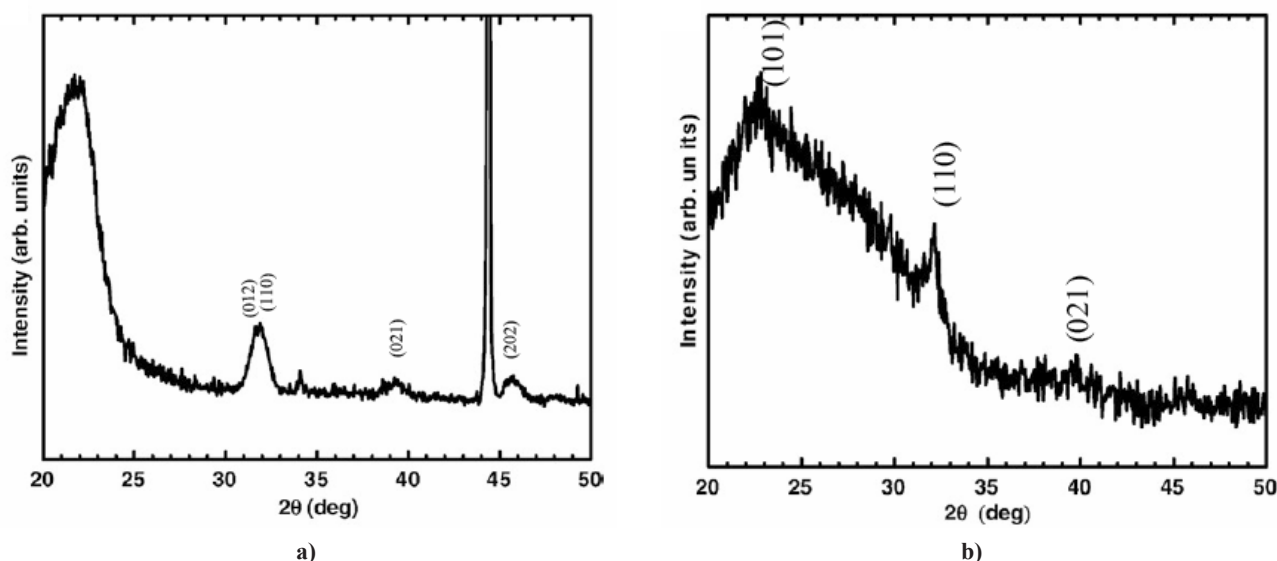


Figure 1. XRD pattern of BiFeO_3 thin films prepared from the Bi-Fe precursor solution with heat treatment at 600°C for 3 h on steel (A) and silica glass (B) substrate [$\text{CuK}\alpha$ radiation ($\lambda=1.5405 \text{ \AA}$)]

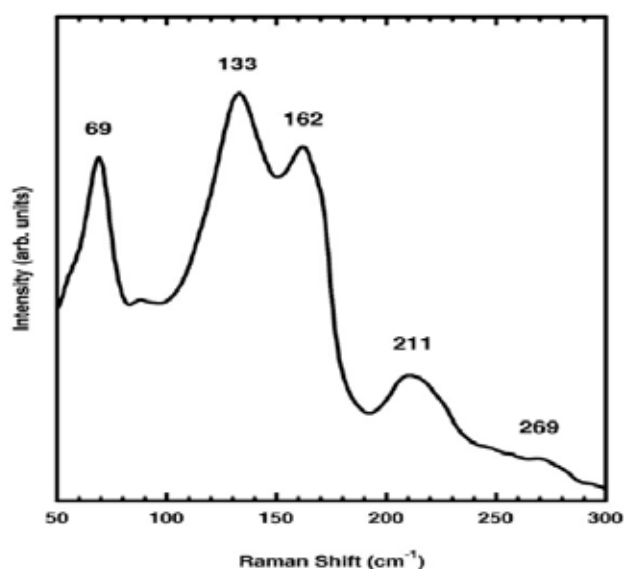


Figure 2. Raman features of the BiFeO_3 film deposited on steel substrate

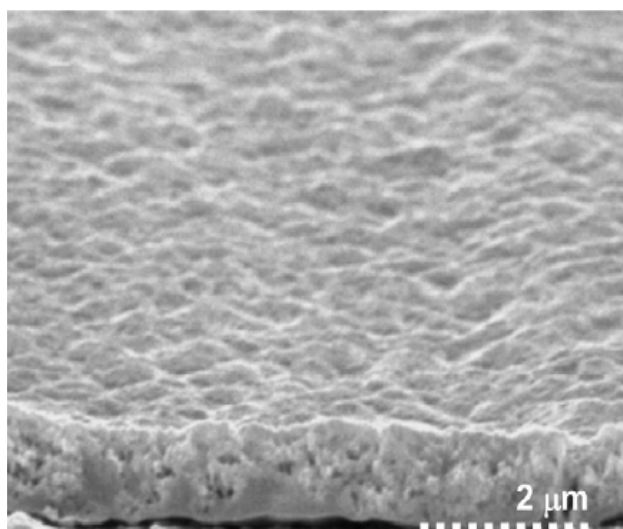


Figure 3. SEM images of the BiFeO_3 film on steel substrate

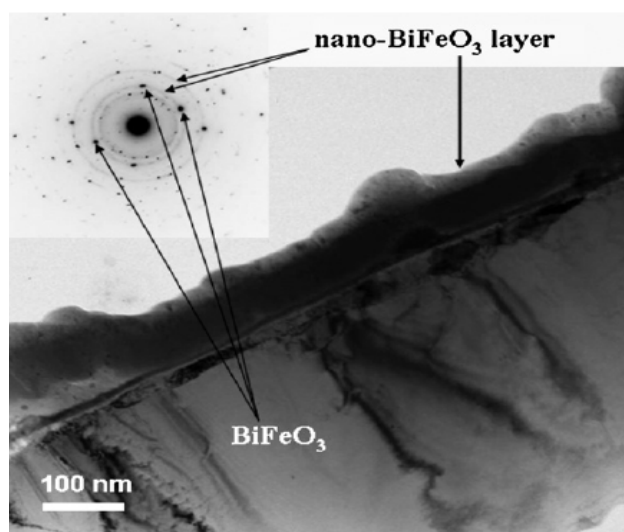


Figure 4. TEM and SAED images showing a cross-section of the BiFeO_3 film

that no impurity phase existed in the film after the treatment at 600°C. The amorphous gel film crystallized to a single phase perovskite with no formation of intermediate phases or unwanted second phases. The XRD coherent crystalline domain size is around 12 nm. When the film was deposited, using the same experimental conditions, on silica optical glass substrate, it exhibited a somewhat lower degree of crystallinity.

The Raman spectroscopy data of the BiFeO_3 thin films crystallized at 600°C for 1 h on stainless steel substrate are in good agreement with the X-ray diffraction pattern, showing that the films are rhombohedrally distorted perovskite BiFeO_3 (Fig. 2). The film shows similar structure to bulk BiFeO_3 material prepared by the same method [25]. Similarly to other reported data [27], our thin films show the presence of the $R3c$ symmetry; the wide bands indicate a small crystalline size.

The XPS experimental data revealed that the 3/2 and 1/2 spin orbit doublet components of the $\text{Fe}2p$ photoemission located at 711.5 and 725.8 eV respectively, were identified as Fe^{3+} . No Fe^{2+} and Fe were found. The XPS results show that BiFeO_3 thin film has a single phase with Fe present in the 3+ valence state, consistent with the Raman and XRD results.

SEM measurements revealed that the BiFeO_3 film was crack free, with a homogeneous thickness. We scratched the surface in order to see the thickness and the transversal microstructure of the film, evidenced in the obtained micrographs taken on samples tilted at an angle almost perpendicular to the electron beam. The morphology is dense and uniform, which further supported the absence of second phases as observed in Raman spectroscopy and XRD. An uniform microstructure and a grain size of less than 50 nm can be noticed (Fig. 3).

TEM images of the BiFeO_3 film show that the BiFeO_3 layer is well-grown and polycrystalline, with a homogeneous thickness and a dense microstructure. The TEM analysis revealed that the film (cross section) consists of two sublayers both, of BiFeO_3 : a nano-layer at the outer surface and a micro-layer below. Selected area electron diffraction measurements indicated the lower crystallinity of the nanolayer (Fig. 4).

The cross sectional TEM measurements of the film confirmed that it is crack-free, dense and polycrystalline. The film deposited on the steel substrate has two sublayers: a very thin (less than 100 nm) nanocrystalline layer, with crystallite size of a few nanometers, and a thicker (less than 1 micron) crystalline layer. EDX spectroscopy analysis in several areas of the film gave in all the analyzed regions an almost equal atomic content of Bi and Fe, within the experimental uncertainty. HRTEM micrograph at the interface between BiFeO_3 and the stainless steel substrate has shown excellent bonding to the substrate (Fig. 5).

From the measurement it becomes clear that this preparation method does not lead to any orientation of

the BiFeO_3 nanocrystallites. The micrograph shows that BiFeO_3 nanocrystallites placed at about 2 nm from the interface are randomly oriented. Some contrast can be observed in a very thin layer of less than 1 nm, at the edge of the stainless steel, indicating that the building up of thermal strains in the steel lattice is limited to a thin region of a few atomic layers.

When the citric acid is replaced by polyvinyl alcohol some changes may be observed. Fig. 6 exhibits room temperature Raman spectra of bulk BiFeO_3 (as obtained), similar to the one reported in reference [28] and of two BFO films on glass substrate obtained with two different chelating agents: polyvinyl alcohol and citric acid [20].

As it could be foreseen, both films have shown similar spectra to bulk BFO material except for some up-shifted frequency peaks and the peak located at about 92 cm^{-1} which seems to decrease drastically for both films. Singh *et al.* [27] assigned the four peaks at 136, 168, 215, 425 cm^{-1} to $A_1(\text{LO-TO})$ modes and the peaks located at 275, 335, 363, 456, 549 and 597 cm^{-1} to $E(\text{TO})$ phonons in polarized Raman spectra on BFO films with $R3c$ symmetry. Due to the reduced intensities and widened peaks one can conclude that the two films have lowered their crystallinity, in comparison to the bulk BiFeO_3 in the following succession: BFO bulk > BFO-SP2 > BFO-SC2.

SE spectra have been fitted using a new model based on multilayer and multicomponent Bruggemann's effective medium approximation (B-EMA) [29]. While the published model [20] consists of a mixture of the dielectric constants of Bi_2O_3 and Fe_2O_3 , this new one included also the dielectric constants of the solution precursors. The following components have been used as references in the simulation program: Bi_2O_3 , a 1 : 1 volumetric mixture of $\text{Bi}(\text{NO}_3)_3$: $\text{Fe}(\text{NO}_3)_3$ termed as Bi+FeNO_3 (see Table 1), $\text{Bi}(\text{NO}_3)_3$, Fe_2O_3 , $\text{Fe}(\text{NO}_3)_3$ and voids. While the dielectric functions of Bi_2O_3 and Fe_2O_3 were taken from literature databases [30], the Bi+FeNO_3 , $\text{Bi}(\text{NO}_3)_3$, and $\text{Fe}(\text{NO}_3)_3$ were measured by a Pulfrich type refractometer.

The volume fractions of the components and the thickness of the layers were used as fitting parameters. Both precursors induce a slightly different behaviour of the films regarding optical constants, films thickness and composition. The citric-type samples lead to films with smaller n , k and d ($n = 1.558$ at $\lambda = 0.55 \mu\text{m}$) and Δd (difference in thickness between the second and the first layer, see Table 1) in the range of 147–200 nm, confirmed also by SEM images, in comparison with the polyvinyl-type samples ($n = 1.604$ at $\lambda = 0.55 \mu\text{m}$ and $\Delta d = 220\text{--}270 \text{ nm}$). These observations were correlated with complementary chemical and structural methods. Detailed XRD analysis has been presented [20] being in good accordance with the above observation.

Data obtained from XPS analysis show that Fe2p as well as Bi4f exhibit typical 3+ oxidation states (Fig. 7) with a lower concentration of Fe^{3+} on the top of the sur-

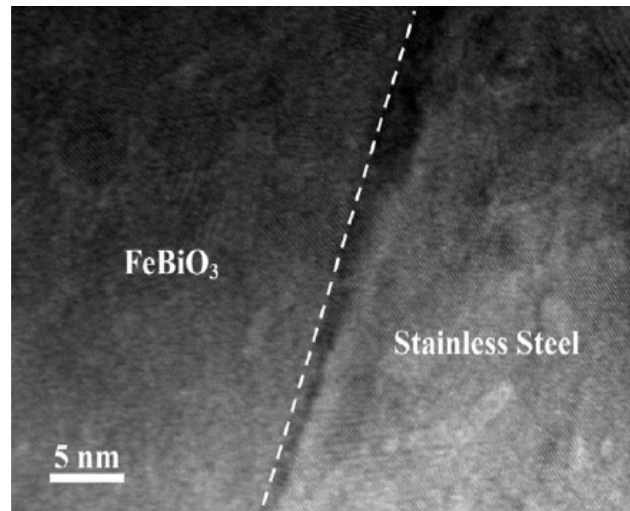


Figure 5. HRTEM image of the BiFeO_3 /stainless steel interface film

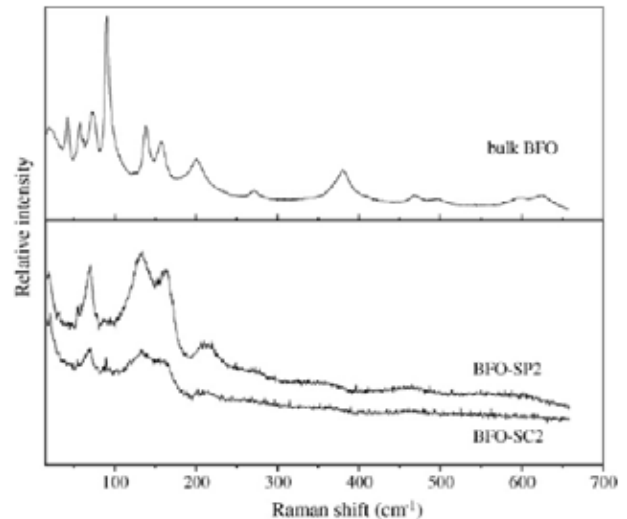


Figure 6. Raman spectra of bulk BiFeO_3 and of two BiFeO_3 films: BFO-SP2 (polyvinyl alcohol) and BFO-SC2 (citric acid)

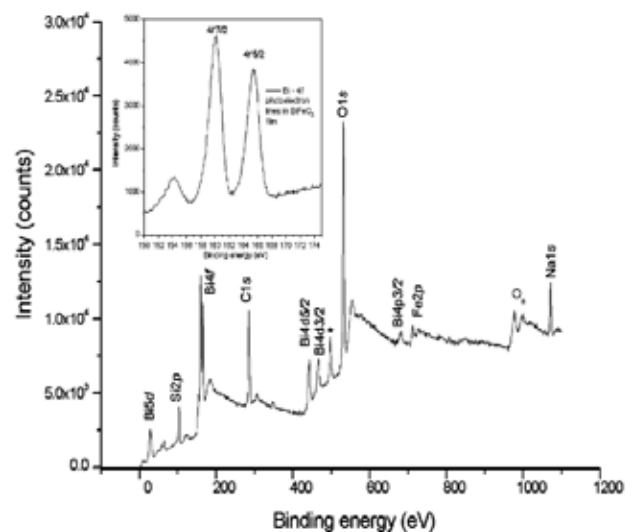
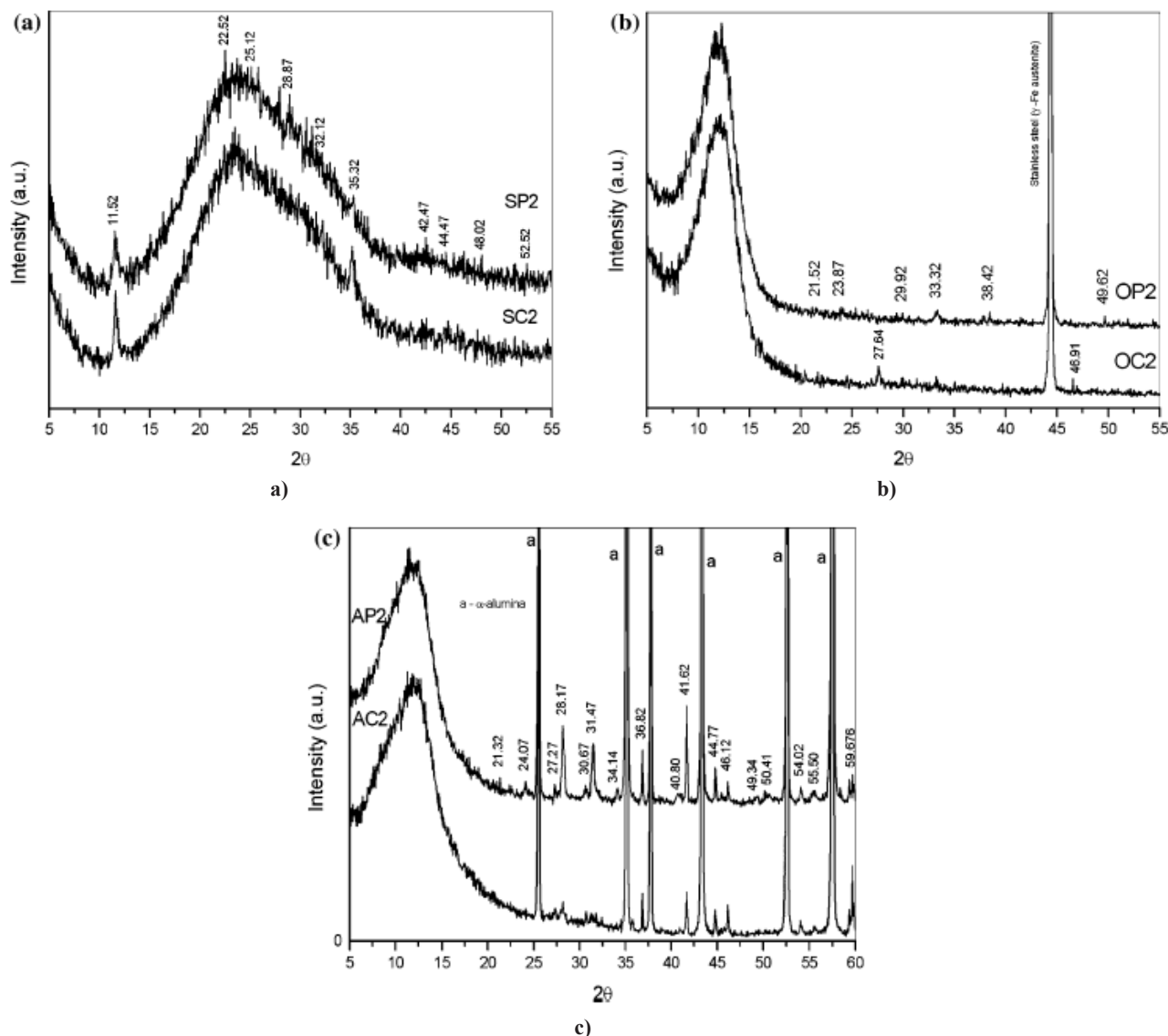


Figure 7. XPS survey of BiFeO_3 two layers films onto a glass substrate annealed 1 h at 500°C . Inset, Bi 4f core-level spectrum (* Satellite line due to oxygen contaminated Al anode)

Table 1. Thickness (d) and volume fractions of the components of BiFeO_3 samples obtained from the best fit of the experimental ellipsometric data

Sample	d [Å]	Bi_2O_3 [%] ^a	Bi+FeNO_3 [%] ^b	$\text{Bi(NO}_3)_3$ [%] ^b	Fe_2O_3 [%] ^a	$\text{Fe(NO}_3)_3$ [%] ^b	Voids [%]	$\Delta d_{(\text{lay1-lay2})}$ [nm]
BFO-C1	1800	8.29	54.78	12.51	12.26	6.16	6.00	208
BFO-C2	3680	11.95	49.24	14.09	12.62	6.30	5.80	
BFO-P1	1080	14.09	51.84	11.67	11.25	5.87	5.27	255
BFO-P2	3630	0.10	63.29	6.05	22.36	4.30	3.90	

^a Optical databases (e.g., <http://www.luxpop.com>).^b Precursors solutions**Figure 8. The XRD patterns of BiFeO_3 films after thermal treatment at 500°C for 1 h on different substrates: glass (a), stainless steel (b) and alumina (c); C-citric acid, P-polyvinyl alcohol [CuK α radiation ($\lambda=1.5405 \text{ \AA}$)]**

face as a result of a possible Bi segregation to the surface.

The XPS sensitivity to the outermost surface layer must be emphasized meaning that only the first 20–30 monolayers (a few nm) can be detected. Carbon is present on the surface as the main contaminant but the detection of Si2p at 102.4 eV together with the appearance of the Na1s at 1072 eV reveals the presence of silicates

from the substrate. It resulted from film nonuniformities and/or imperfections. Oxygen O1s (530.7 eV) is bonded mostly to Bi^{3+} .

After the thermal treatment the films morphology is changed with a continuous variation in the volume fractions of the components, optical constants (n and k) and thickness. Both C- (citric acid) and P-type (polyvi-

nyl alcohol) samples become denser, as the voids content decreases, which exhibit a clear tendency of crystallization but smaller than in the case of bulk BiFeO_3 - revealed by Raman results. In this respect, the following succession was found: (BFO bulk) > (BFO-C2) > (BFO-P2). In the near surface region one may notice the lower relative concentration of Fe, suggesting a possible Bi segregation to the surface and/or Fe diffusion into film.

Thin films of bismuth ferrite, obtained by a wet chemical low-temperature process, using bismuth and iron nitrates and two chelating agents (citric acid and polyvinyl alcohol) were successively deposited on different types of substrates (silica glass, steel and sintered

alumina) by the immersion technique [31].

The detailed XRD spectra corresponding to the specimens deposit on glass (a), stainless steel (b) and alumina (c) are shown in Fig. 8. It can be seen that at lower temperature the formed phases are strongly influenced by the nature of the chelating agent and the type of substrate. Bismuth oxide is formed especially on the glass substrate and subsequently $\text{Bi}_{36}\text{Fe}_2\text{O}_{36}$ appears especially on the film surface. The presence of BiFeO_3 formed at this temperature may be inferred by some diffraction lines which can be assigned to a distorted perovskite structure. The process of BiFeO_3 formation is not finished in the investigated conditions. These observations are in accordance with the previous investigation on Bi_2O_3 and BiFeO_3 films formation [19,20].

Fig. 9 shows room temperature Raman spectra of bulk BiFeO_3 and of the BFO films on glass, stainless steel and alumina obtained using the two chelating agents.

Polyvinyl alcohol caused wider bands and higher Raman peak intensities compared to those obtained using citric acid. There is a peak intensity decrease from the glass substrate toward the steel substrate (Fig. 9b). Similar behaviour shows the films with polyvinyl alcohol, on all substrates except the one on alumina. Both films on stainless steel, OC2 and OP2 show distinct spectral features over 250–450 cm^{-1} . In this spectral range there are few peaks, except for the peak at 380 cm^{-1} , originating from residual Fe_2O_3 and/or from the stainless steel substrate [32]. Higher frequency peak position of both films can point out a higher distorted R3c phase and/or the formation of a second phase, $\text{Bi}_{36}\text{Fe}_2\text{O}_{57}$ as reported earlier [33]. Since the processing temperature of the films was kept around 500°C and the thermal stability range of $\text{Bi}_{36}\text{Fe}_2\text{O}_{57}$ is about 600–700°C, a possible explanation consists in the presence of some residual Bi_2O_3 and Fe_2O_3 as well as of small amounts (under X-ray detection limit) of the $\text{Bi}_{36}\text{Fe}_2\text{O}_{57}$ phase (XPS identified) in both films.

2.2 BiFeO_3 powders

The interest in the investigation of the BiFeO_3 as a bulk material is justified by the need to distinguish between the intrinsic and extrinsic contributions to the electrical characteristics of this material. It is expected that in films, particularly in ultrathin structures, extrinsic factors such as epitaxial stresses, electrode film or intergrain interfaces play an important role on the electrical properties of the system. In this spirit, the bulk polycrystalline ceramic is an isotropic system in which the electrode material interfaces give a negligible contribution to the total impedance, so that values closer to the intrinsic ones are expected for the electrical properties [34]. During synthesis, the kinetics of formation always leads to a mixture of BiFeO_3 as a major phase along with other impurity phases. The task becomes dif-

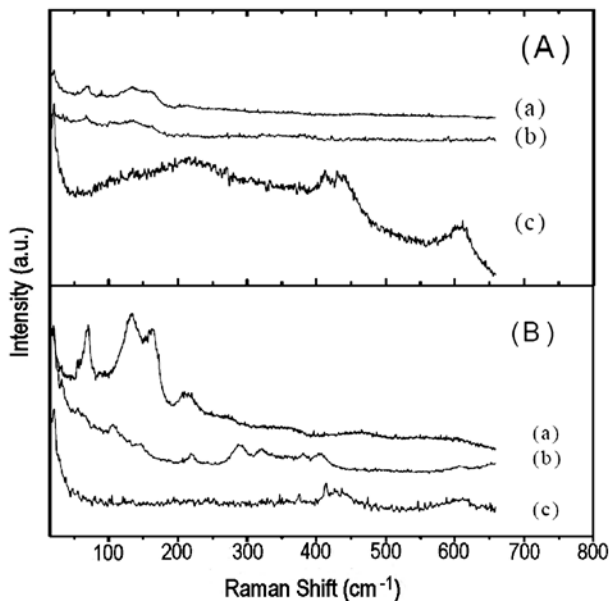


Figure 9. Raman spectra of the BiFeO_3 films obtained by using two chelating agents: (A) citric acid and (B) polyvinyl alcohol on different substrates: glass (a), stainless steel (b) and alumina (c)

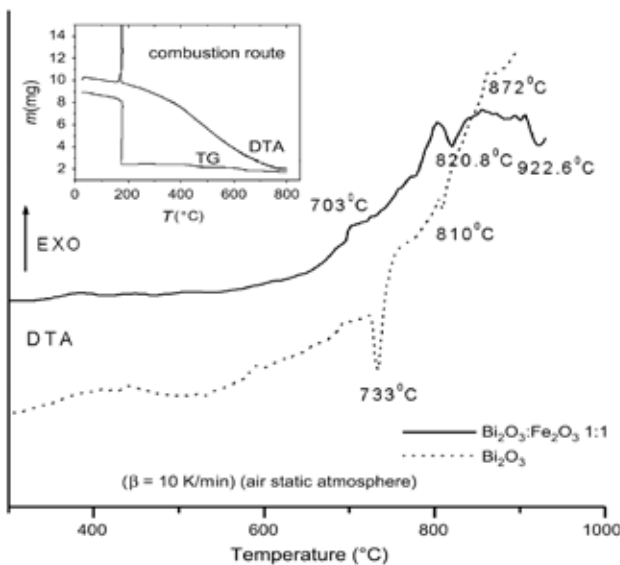


Figure 10. DTA curves of $\text{Bi}_2\text{O}_3:\text{Fe}_2\text{O}_3$ 1:1 mixture and nitrates precursor (insert)

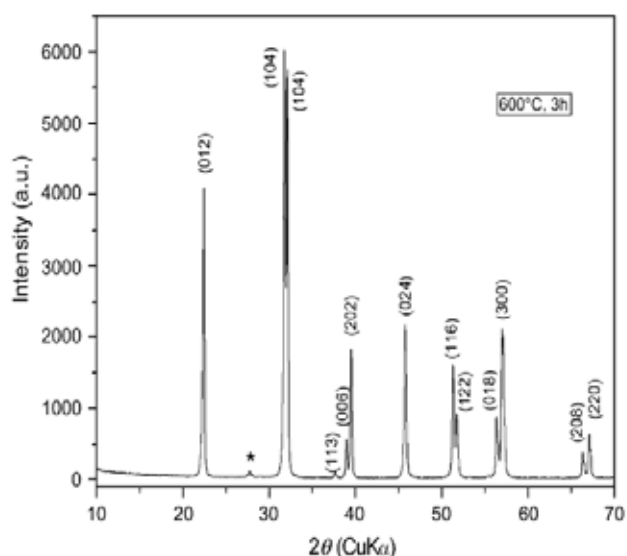


Figure 11. XRD patterns of BiFeO_3 nanopowder obtained by combustion route (* secondary phase) [CuK α radiation ($\lambda=1.5405 \text{ \AA}$)]

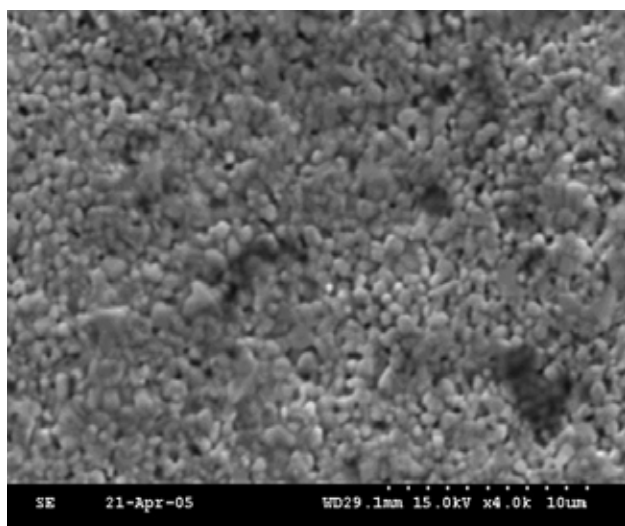


Figure 12. SEM micrographs of BiFeO_3 sample sintered at $700^\circ\text{C}/1\text{h}$ (combustion route)

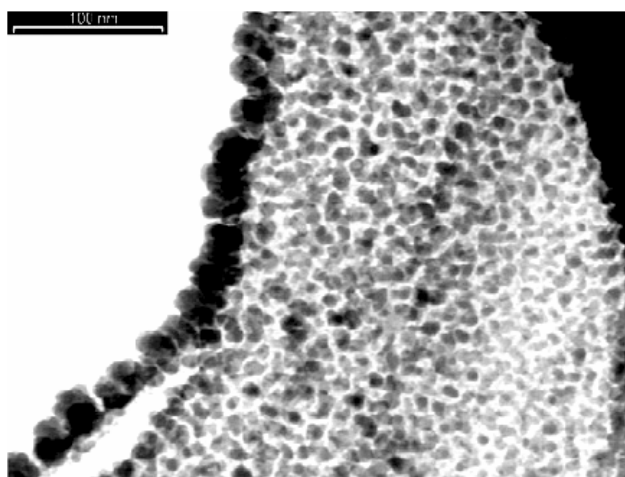


Figure 13. TEM images of BiFeO_3 sample annealed at $700^\circ\text{C}/3\text{h}$ obtained by combustion technique

difficult because of the narrow temperature range in which BiFeO_3 stabilizes and there are a number of other phases of Bi and Fe, which appear if the temperature is not controlled accurately. Several authors [35] have reported the existence of $\text{Bi}_2\text{Fe}_4\text{O}_9$ or $\text{Bi}_{46}\text{Fe}_2\text{O}_{72}$ as an additional impurity phase in spite of adopting the improvised method suggested by Sosnowska *et al.* [36] and Achenbach *et al.* [37]. Another method include simultaneous precipitation/coprecipitation involving Bi and Fe nitrates starting solutions as treated with ammonium hydroxide and thermal treatments at $550\text{--}750^\circ\text{C}$ to get a pure BiFeO_3 phase [38]. The synthesis of pure BiFeO_3 powder was reported consisting of a solution evaporation process at a temperature as low as 400°C , using the corresponding nitrates but dissolved in a strong acid such as nitric acid 2N [39]. Fruth *et al.* [24,40] reported the preparation of bismuth ferrite by the solution combustion method from an α -alanine containing precursor. As reference, BiFeO_3 was prepared by the conventional classic ceramic route starting from Bi_2O_3 and Fe_2O_3 (99% in purity). Fig. 10 presents the differential thermal analysis (DTA) curves of $\text{Bi}_2\text{O}_3 : \text{Fe}_2\text{O}_3$ 1 : 1 mixture compared with bismuth sesquioxide (dotted line) and BiFeO_3 α -alanine-based precursor (see inserted picture). Only a highly exothermic effect with a major weight loss in the $157\text{--}177^\circ\text{C}$ temperature range for the last case can be noticed. An endothermic event at around $710\text{--}730^\circ\text{C}$, characteristic to the α/δ Bi_2O_3 polymorph transition was observed but the endothermic event at 810°C on the Bi_2O_3 DTA curve, assigned to the melting of this oxide is missing. This observation suggests that the reaction between the components is very fast and started at lower temperatures. Also the absence of the endothermic effect at 810°C , assigned to the melting of Bi_2O_3 , proves that this component has already reacted. Based on this observation we have established the corresponding annealing treatments.

XRD patterns for BiFeO_3 powders obtained after 3 h of annealing at 600°C , in air revealed that BiFeO_3 is obtained at low temperature with rhombohedral distorted perovskite structure with $a_{\text{hex}} = 5.577 \text{ \AA}$ and $c_{\text{hex}} = 13.866 \text{ \AA}$ (Fig. 11). In the case of the classic route ($800^\circ\text{C}/1 \text{ h}$) the cell parameters were $a_{\text{hex}} = 5.570 \text{ \AA}$ and $c_{\text{hex}} = 13.861 \text{ \AA}$ in accordance with the size effect studies of BiFeO_3 which indicate that as the particle size decreases, the lattice expands [41]. A trace of a bismuth rich secondary phase (silenite-type) was observed. The intensity of the secondary phase peak at $2\theta = 27.9^\circ$ is the highest for the samples obtained by calcining the precursor at 500°C for 3 h and decreases in the case of the samples obtained at 600°C .

SEM (Fig. 12) and TEM images (Fig. 13) confirm the above observations. After sintering the nanopowder at $700^\circ\text{C}/1 \text{ h}$ (Fig. 12), a high tendency of densification can be observed. A high interconnection of the grains can be noticed and also the presence of small amounts

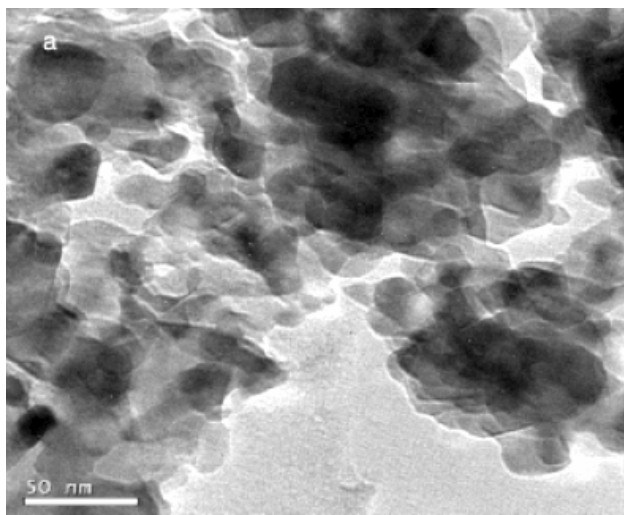


Figure 14. TEM images of the precursor powder

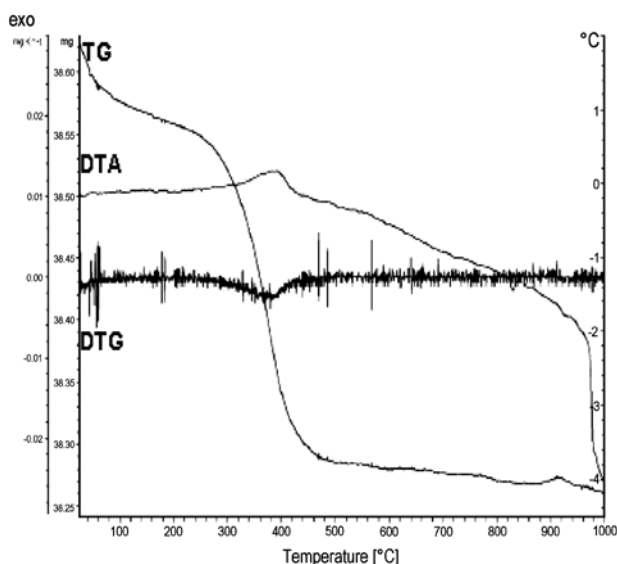


Figure 15. The thermal analysis results for the BiFeO_3 powder precursor, treated in air between 20–1000°C

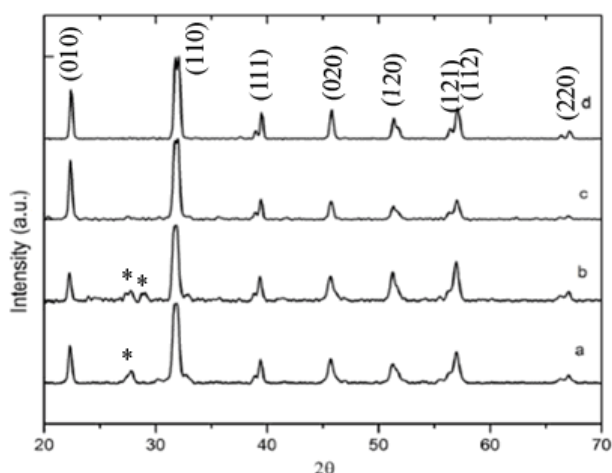


Figure 16. The X-ray diffraction patterns of the BiFeO_3 powders crystallized at different temperatures
a) 350°C, b) 400°C, c) 500°C, d) 600°C
[CuK α radiation ($\lambda=1.5405 \text{ \AA}$)]

of a secondary phase.

Popa *et al.* [25] reported a simple technique for the preparation of single phase BiFeO_3 powders using the polymerized complex method, starting from iron and bismuth nitrates. A mixed aqueous solution with citric acid (CA), ethylene glycol (EG), Bi and Fe ions was polymerized. The initial powder images indicate that the onset crystallization occur already around 350°C. It can be observed that crystalline grains were already formed at this temperature in the precursor powder and show small particle size around 20 nm (Fig. 14).

A broad exothermic effect on the DTA curve (Fig. 15) associated with a major weight loss on the TG curve, at around 380°C, can be assigned to the decomposition of the trapped nitrates and noticed up to 900°C. At around 935°C, on the DTA curve, there is an endothermic effect caused most probably by the melting of BiFeO_3 . One assumes that the effect at 370°C is also related to the Neel temperature of BiFeO_3 corresponding to the magnetic phase transition of BiFeO_3 [33,42,43].

The XRD data show that the powders were rhombohedrally distorted BiFeO_3 -perovskite, according to JCPDS 20-169 file. The XRD analysis showed that no impurity phases existed in the powders obtained at 600°C (Fig. 16). The initial material was partially crystallized, indicating that the onset crystallization occurs around 350°C, as at this temperature the BiFeO_3 phase begins to form. It can be noticed that in spite of the presence of a Bi rich secondary phase peaks around 27° (marked as * in Fig. 16) completely disappeared at 600°C. Contrary to the observations reported by Ghosh *et al.* [44] related to the use of citric acid replacing tartaric acid in their synthesis method, in this case BiFeO_3 was the only formed phase and no other secondary phases were registered in the final XRD pattern.

Fig. 17 shows the microstructures of the perovskite type BiFeO_3 prepared by PC method at 400 and 500°C. The mean particle size is almost in the nanometric range, between 100–200 nm. The SEM images show an uniform grain size distribution and homogeneous structure. No significant growth of particle size was noticed with the increase of the temperature of the thermal treatment.

III. LaCoO_3 type perovskites

The mixed oxides type perovskite with general formula ABO_3 can be considered strategic materials due to their magnetic, electrical and catalytic properties [45]. Special attention was given to LnMeO_3 type oxides with perovskite structure, where Ln belongs to the lanthanides group and Me is an element of transitional metal groups, due to their application as materials for electrodes in solid electrolyte cells (SOFC) or materials for chemical sensors. LaCoO_3 compound belongs to this class of materials showing interesting electrical and catalytic properties, due to a high ionic and electronic

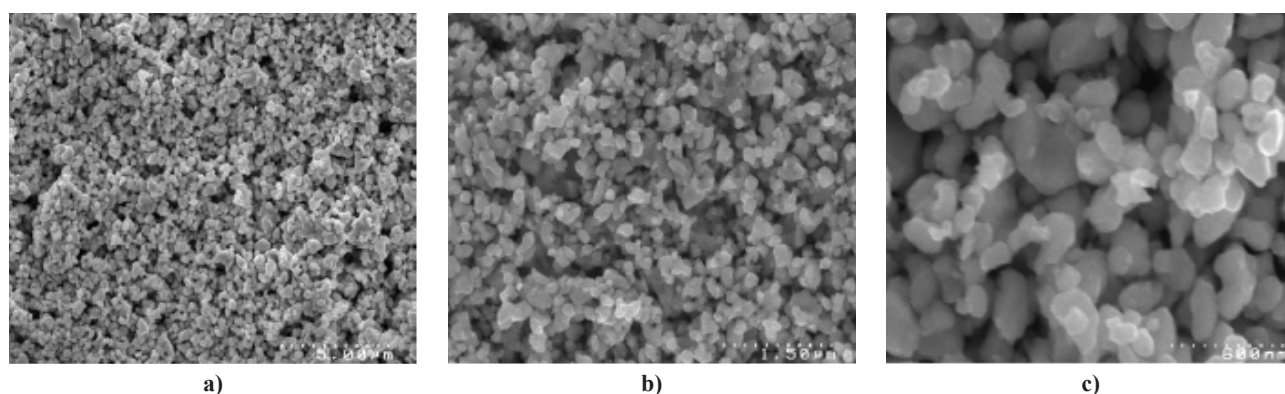


Figure 17. SEM micrographs of the BiFeO_3 perovskite powders at 400°C (a) and 500°C (b, c)

conductivity.

It is also known that LaCoO_3 electrode offers much better performance than the cathode materials based on $\text{LaMnO}_{3+\delta}$ [46,47]. To get good performance and functional properties, dense materials with a well defined microstructure are desired. For this purpose, it is important to prepare high quality powders with controlled microstructure and stoichiometry. Single phase materials are preferred because in most cases, the presence of secondary phases decreases the functional properties. Many authors were interested to synthesize powders or films in this system [3,46–57].

LaCoO_3 compound can be obtained through several methods of preparation. As conventional preparation technique, solid state reactions based on metal oxides, carbonates or oxalates followed by a thermal treatment around 1000°C, with intermediate grinding was used [47]. This method leads to materials with low specific surface area, with low activity, requiring high temperatures and long thermal treatment.

To avoid the disadvantages described above, several new methods were developed, especially techniques in solution, which lead to improved conditions for obtaining pure phases. Such syntheses require low reaction temperatures and enable obtaining homogeneous and fine powders [3].

These methods include the sol-gel process (alkoxide route and aqueous route) in the presence of citrate or tartrate [7], hydrothermal and coprecipitation [58–60].

Kleveland *et al.* [51] used a chemical route starting with nitrates and ethylenediamine tetracetic acid, while Faaland *et al.* [61] applied a spray pyrolysis method start-

ing with the same precursors. Berger *et al.* [62] proposed a combustion method, while Li *et al.* [63] presented a combined method of milling nitrates with nitric acid followed by coprecipitation with potassium hydroxide.

The sol-gel method using alkoxides $\text{La}(\text{O}_i\text{Pr})_3$ and $\text{Co}(\text{NO}_3)_2$ as precursors was used by Hwang [50]. The polymerizable complex method was used by Popa [64] and Guo [65]. The carboxylic route was applied by Taguchi *et al.* [66] and Ajami *et al.* [67] using lanthanum and cobalt nitrate and citric acid as chelating agent.

3.1 LaCoO_3 powders

Sol-gel method is often used as a technique for the preparation of powders, because of well known advantages such as an easy way to obtain homogenous distribution of precursors with the possibility of controlled introduction of a given quantity of dopant, control by chemical reaction, control of viscosity and low temperature of processing. Citrate sol-gel process route presents advantages over other methods not only of good mixing of the components at the atomic scale, but also offers the possibility of obtaining films and fibers which have technological importance [9].

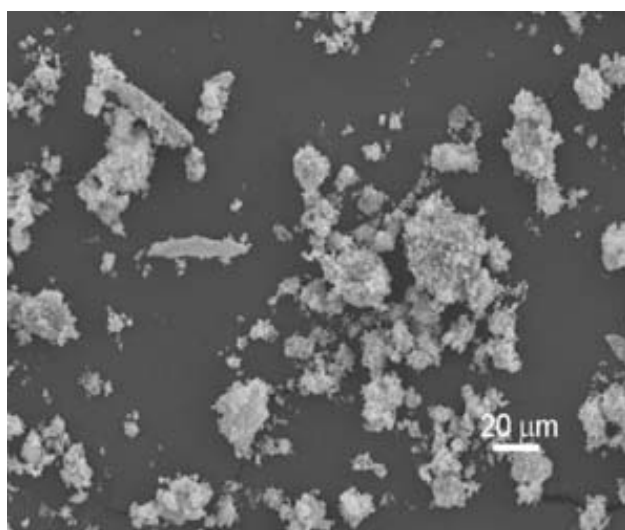
The studies of the LaCoO_3 powder formation started with the investigation of the sol-gel process in aqueous medium using inorganic salts and carboxylic acids (citric acid) as chelating agents [68]. Two different reagents, namely La- and Co nitrates and acetates, respectively and citric acid in 1 : 1 : 1 molar ratio in aqueous solutions were used [69–71]. The solutions, the resulting gels and the powders, starting with nitrate were labelled (N), while the similar solutions and gels

Table 2. The maxima of absorbance identified in the UV-VIS spectra of the studied solutions with their assignments

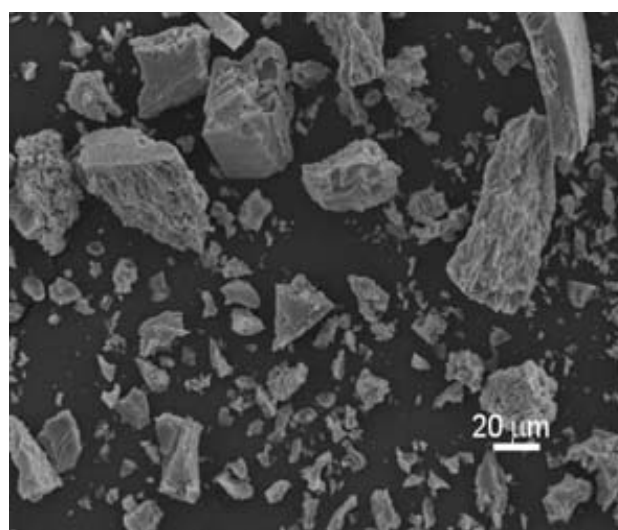
Sample	Maxima of absorbance nm (cm^{-1})	Assignments
La-Co-CA (N) solution	300 nm (33231 cm^{-1})	CT
	468 nm (21368 cm^{-1})	Splitting
	510 nm (19531 cm^{-1})	${}^4T_{1g} \rightarrow {}^4T_{1g}(\text{P})$
La-Co-CA (A) solution	467 nm (20217 cm^{-1})	Splitting
	512 nm (18587 cm^{-1})	${}^4T_{1g} \rightarrow {}^4T_{1g}(\text{P})$

Table 3. The assignment of the vibration bands in IR spectra of the studied solution and gels

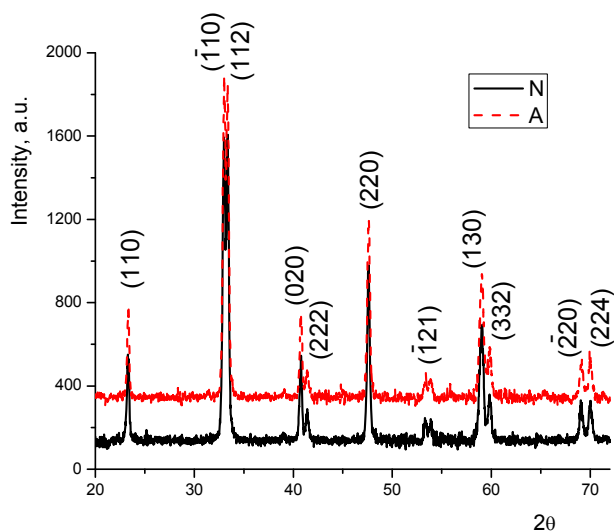
N		A		Vibration mode	Assignments
solution	gel	solution	gel		
3300	3350	3276	3326 3200	ν OH	structural OH group
1718	1720	-	-	ν_{asym} (COO)	carbonyl asymmetric stretching
1635	1616	1636	1616	$\delta_{\text{H}_2\text{O}}$	adsorption of water
-	-	1552	1568	ν_{asym} (COO)	carbonyl asymmetric stretching
1404	1432	1410	1415	ν_{sym} (COO)	carbonyl symmetric stretching
1333	1383	-	-	$\nu_{\text{NO}_3^-}$	introduced by the precursors
1230		1229	1263	$\nu_{\text{C-O}}$	
-	1078	-	1078	π_{CH}	introduced by the citric acid
-	1033	-	1036	$\nu_{\text{C-OH}}$	
-	813	-	912	ν_{CH_2}	



a)



b)

Figure 18. SEM images of the thermally treated samples at 600°C, a) nitrate and b) acetate**Figure 19.** XRD patterns of the LaCoO_3 powder and sintered pellets at 600°C [CuK α radiation ($\lambda=1.5405 \text{ \AA}$)]

obtained with acetates were labelled (A).

The gelling process in the studied solutions was approached by spectroscopic methods. In the UV-VIS spectra of the La-Co solutions based on nitrates and acetates immediately after their preparation and after 30 hours of storage at 80°C the Co^{2+} ions in octahedral coordination were observed [72]. The positions of the absorbance bands of the UV-VIS spectra are presented in Table 2.

In the Table 3 the assignment of the vibration mode in the FT-IR spectra of the same solutions are presented. In the case of the La-Co solutions based on nitrates, according to the frequency separation between the antisymmetric stretching and symmetric stretching of the carbonyl ion ($\Delta\nu = 314 \text{ cm}^{-1}$), it could be concluded that the carboxylic groups of the citrate act as unidentate ligands [73]. On the other hand in the case of La-Co solutions based on acetates the same separation is only $\Delta\nu = 142 \text{ cm}^{-1}$, leading to the conclusion that carboxylic groups of citrate ligands act as bridging ligands.

According to the literature data, systematic investi-

Table 4. The maxima of absorbance identified in the UV-VIS spectra of the studied gels with their assignments

Sample	Maxima of absorbance nm (cm ⁻¹)	Assignments
La-Co-AC (N) gel	356 nm (28089 cm ⁻¹)	CT
	406 nm (24639 cm ⁻¹)	${}^4T_{1g} \rightarrow {}^4A_{2g}$
	532 nm (18797 cm ⁻¹)	${}^4T_{1g} \rightarrow {}^4T_{1g}(P)$
	671 nm (14903 cm ⁻¹)	${}^4T_{1g} \rightarrow {}^4B_{1g}$
La-Co-AC (A) gel	372 nm (26881 cm ⁻¹)	CT
	540 nm (18518 cm ⁻¹)	${}^4T_{1g} \rightarrow {}^4T_{1g}(P)$
	685 nm (14598 cm ⁻¹)	${}^4A_{2g} \rightarrow {}^4T_{1g}(P)$

Table 5. Crystallographic parameters, particle size and internal stress of the thermally treated powders at 600°C

Sample	<i>a</i> [Å]	<i>c</i> [Å]	<i>c/a</i>	<i>V</i> [Å ³]	<i>S</i> [E ⁻³]	<i>D</i> [Å]	BET surface area [m ² /g]
LaCoO ₃ (N)	5.4390	13.1616	2.4199	337,19	0.87	537	8.82
LaCoO ₃ (A)	5.4455	13.2098	2.4258	339.24	1.04	777	13.30

Table 6. Ceramic properties of the sintered samples at different temperatures

Sintering temperature [°C]	Shrinkage Δl/l [%]	Open porosity %	Experimental density [g/cm ³]	Relative density [%TD]
Sintered samples from powders obtained from nitrates				
800	1.65	7.12	4.92	73
900	6.00	5.29	6.14	91
1000	10.60	4.77	6.34	94
1100	15.50	1.29	6.50	96
1200	18.85	0.12	6.71	99
Sintered samples from powders obtained form acetates				
800	6.9	6.09	3.88	58
900	10.45	9.36	5.11	76
1000	13.00	5.68	5.66	84
1100	19.25	2.58	5.81	86
1200	24.30	1.31	6.21	92

gations of the sol-gel chemistry in the aqueous medium using citric acid for the mentioned system have not been carried out before.

The viscosities of solutions kept at 80°C display a slow constant continuous growing evolution in time. For the solutions prepared starting with acetates a higher viscosity was observed relatively to the solution starting from nitrate, due to the presence of the acetate ions which can act also as a chelating agent. The increase of the viscosity values takes place between 1.7 cP and 2.05 cP for the nitrate derived solution and 1.75 cP and 2.25 cP for the acetate derived solution.

Under above presented experimental conditions amorphous red gels were obtained.

The SEM images of the samples obtained with different starting precursors (nitrate N and acetate A), are presented in Fig. 18 and show pieces of gel. The sizes of the gels' fragments are different and depend on the

starting precursors.

The positions of the absorbance bands of the UV-VIS spectra, of gels obtained starting with nitrates and acetates are presented in Table 4. In the spectrum of the nitrate-derived gel the d-d transitions correspond to the Co(II) ion in the tetragonal distorted geometry. In the acetate-derived gel the d-d transitions correspond to the formation of complex gels in which Co(II) ion has an octahedral symmetry.

Based on the data presented above one may conclude that during the sol-gel processes of the lanthanum-cobalt-citric acid system in the presence of the carboxylic acids starting with both nitrates and acetates, a lanthanum cobalt citrate gel with a coordinative structure was obtained.

The thermal behaviour of the dried gels was also investigated. Both dried gels lose weight stepwise. The choice of the starting compounds influences the path-

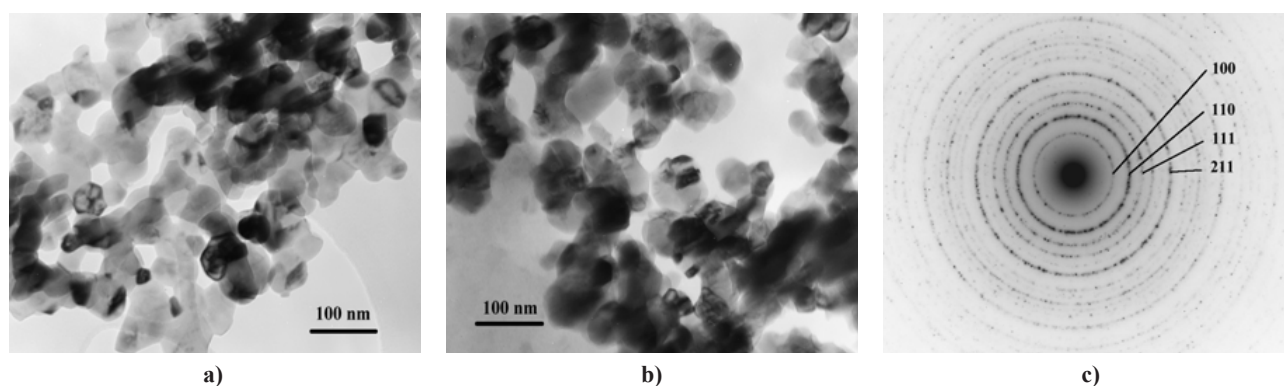


Figure 20. TEM and SAED images of the LaCoO_3 , powders thermally treated at 600°C , a) starting with nitrate, b) starting with acetate and c) SAED for sample a [68]

way of decomposition. Above 400°C for nitrate-based and above 500°C for acetate based gels there is no pronounced weight loss [71].

According to the results obtained by DTA/TG analysis, the gels were thermally treated at 600°C , for 6 hours leading to the formation of the single pure perovskite rhombohedral phase of LaCoO_3 (JCPDS 84-0848) (Fig. 19). The annealed samples were evaluated by X-ray diffraction using a $\text{CuK}\alpha$ ($\lambda = 0.1540 \text{ nm}$) radiation source in a BRUKER AXS D4 ENDEAVOR X-ray diffractometer. The diffraction angle (2θ) range between 10° and 90° was scanned.

In Table 5 the XRD evaluation of the crystallographic parameters, particle size and internal stress of the thermally treated powders is presented.

The presented results have shown the same rhombohedral perovskite structure for both samples, but with higher values of the crystallographic parameters, higher internal stress of the crystals, higher particles size and higher surface area when acetates were used as precursors. Due to the fact that in the case of the powders obtained from acetates both particles size and specific surface area are higher than in the case of the powders obtained from nitrates, one may assume that in this latter case an intragranular porosity is present.

TEM and SAED measurements confirm the for-

mation of the rhombohedral perovskite structure of the LaCoO_3 (Fig. 20) which is in accordance with the XRD results.

Comparing our data with results published before, one may underline that the formation of LaCoO_3 powder, as pure phase, takes place at essentially lower temperature as the previously published [51,74].

3.2 LaCoO_3 ceramic samples

According to the literature data no matter of the precursor powders used, the sintering temperature and time required for obtaining dense ceramic samples were high. Schmidt *et al.* [74] obtained sintered samples by thermal treatment at 1200°C for one day, starting with powders prepared by classical method, while Kleveland *et al.* [51] used the same procedure with powders obtained by chemical methods.

Preoana *et al.* [75] studied the sintering properties of the pressed powders characterized above in the temperature range $800\text{--}1200^\circ\text{C}$. The ceramic properties of the pressed and sintered samples are presented in Table 6. One may notice that the variation of the open porosity with the thermal treatment of the samples obtained from both powders presents close values. However, the ceramics obtained from the powders prepared from acetates have shown much lower densities as compared with

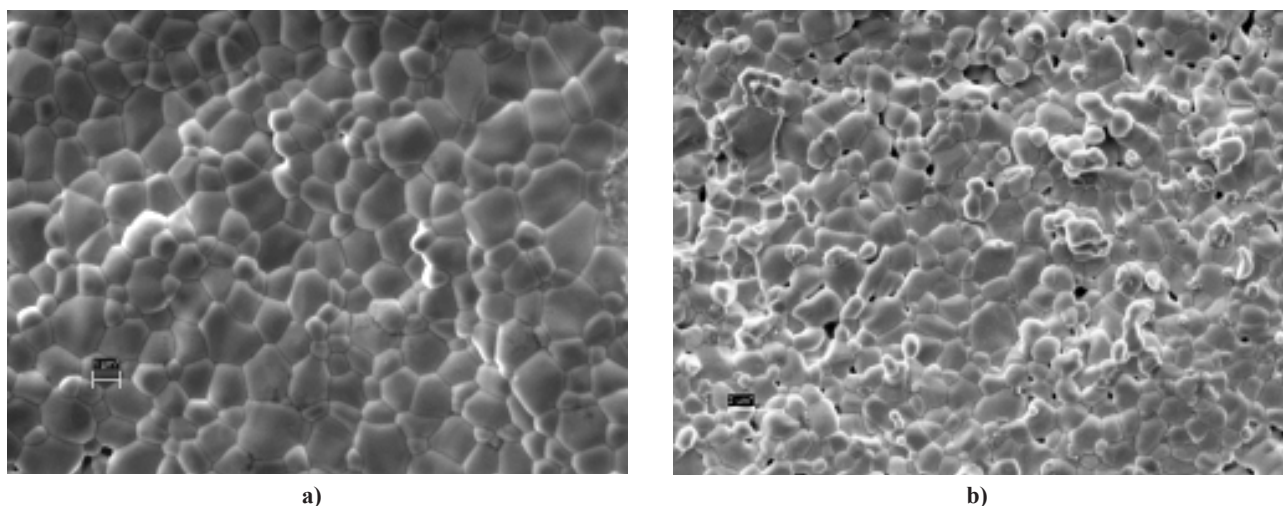


Figure 21. SEM images of the samples sintered at 1100°C , a) nitrate and b) acetate

the powder samples prepared from nitrates. This behaviour could be correlated to the presence of an internal porosity of the grains obtained starting with acetates.

The structure of the sintered powders, as determined by XRD was the same as in the initial powders, but with a higher intensity of the diffraction lines. In the case of the powders obtained starting with acetates, Co_2O_3 traces occurred during the sintering process at highest temperature (1200°C), as a secondary phase.

The SEM images (Fig. 21) have shown a lower tendency for sintering and a less homogeneous morphology for the ceramics prepared from powders obtained from acetates.

The ceramics sintered at 1100°C from powders obtained from nitrates present uniform grain size distribution and practically no open porosity.

The increased sintering ability of the reactive powders obtained by innovative methods lead to ceramic bodies with good ceramic properties at lower temperature than that reported before (1100°C as compared to 1250°C).

IV. Conclusions

In the present review results concerning the preparation of two type of perovskite, namely FeBiO_3 and LaCoO_3 , by chemical innovative methods are presented. The structural properties of films, powders and sintered bodies are also discussed. The beneficial effect on the preparation methods used on the structure and properties of the resulted materials is revealed.

Acknowledgements: In the presented review results obtained during the COST Action 539 are discussed. The authors acknowledge the fruitful collaboration with the partners in the action and its financial support.

References

1. W.D. Kingery, H.K. Bowen, D.R. Uhlmann, *Introduction to Ceramics*, Wiley, New York, 1976.
2. C.J. Brinker, G.W. Scherer, *Sol-Gel Science: The Physics and Chemistry of Sol-Gel Processing*, Academic Press, San Diego, 1990.
3. E. Traversa, P. Nunziante, M. Sakamoto, Y. Sadaoka, R. Montanari, "Synthesis and structural characterization of trimetallic perovskite-type oxides $\text{LaFe}_x\text{Co}_{1-x}\text{O}_3$ by the thermal decomposition of Cyano complexes $\text{La}[\text{Fe}_x\text{Co}_{1-x}(\text{CN}_6)] \cdot n\text{H}_2\text{O}$ ", *Mater. Res. Bull.*, **33** [5] (1998) 673–681.
4. M. Kakihana, "Sol-gel preparation of high temperature superconducting oxides", *J. Sol-Gel Sci. Technol.*, **6** (1996) 7–55.
5. I. Lazău, Z. Ecsedi, C. Păcurariu, R. Ianoș, *Metode conventionale utilizate în sinteza compușilor oxidici*, Editura Politehnică, Timișoara, 2006.
6. W.L. Suchanek, R.E. Riman, "Hydrothermal synthesis of advanced ceramic powders", *Adv. Sci. Techn.*, **45** (2006) 184–193.
7. E. Campagnoli, A. Tavares, L. Fabbrinu, I. Rossetti, Yu.A. Dubitsky, A. Zaopo, L. Forni, "Effect of preparation method on activity and stability of LaMnO_3 and LaCoO_3 catalysts for the flameless combustion of methane", *Appl. Catal. B: Environ.*, **55** (2005) 133–139.
8. H. Schmidt, A. Seferling, "Chemistry and applications of inorganic-organic polymers (Organically modified silicates)", *Mater. Res. Soc.*, 739 (1986) 739–750.
9. C.C. Chen, C.H. Shen, R.S. Liu, J.G. Lin, C.Y. Huang, "Synthesis and characterization of the colossal magnetoresistance manganite $\text{La}_{1.2}(\text{Sr}_{1.4}\text{Ca}_{0.4})\text{Mn}_2\text{O}_7$ by citric gel", *Mater. Res. Bull.*, **37** (2002) 235–246.
10. A.C. Pierre, *Introduction to the sol-gel process*, Kluwer Academic Publishers, Boston, 1998.
11. L.G. Sillén, "Quantitative studies of hydrolytic equilibria", *Quart. Rev. Chem. Soc.*, **13** (1959) 146–168.
12. J. Livage, M. Henry, C. Sanchez, "Sol-gel chemistry of transition metal oxides", *Progr. Solid State Chem.*, **18** (1988) 259–341.
13. J. Wang, J.B. Neaton, H. Zheng, V. Nagarajan, S.B. Ogale, B. Liu, D. Viehland, V. Vaithyanathan, D.G. Schlom, U.V. Waghmare, N.A. Spaldin, K.M. Rabe, M. Wuttig, R. Ramesh, "Epitaxial BiFeO_3 multiferroic thin film heterostructures", *Science*, **299** (2003) 1719–1722.
14. J. Wang, A. Scholl, H. Zheng, S.B. Ogale, D. Viehland, D.G. Schlom, N.A. Spaldin, K.M. Rabe, M. Wuttig, L. Mohaddes, J. Neaton, U. Waghmare, T. Zhao, R. Ramesh, "Response to comment on "Epitaxial BiFeO_3 multiferroic thin film heterostructures". *Science*, **307** (2005) 1203b.
15. R. Ramesh, N.A. Spaldin, "Multiferroics: Progress and prospects in thin film", *Nat. Mater.*, **6** (2007) 21–20.
16. R.W. Schwartz, "Chemical solution deposition of perovskite thin films", *Chem. Mater.*, **9** (1997) 2325–2340.
17. H. Liu, Z. Liu, Q. Liu, K. Yao, "Ferroelectric properties of BiFeO_3 films grown by sol-gel process", *Thin Solid Films*, **500** (2006) 105–111.
18. J.K. Kim, S.S. Kim, W-J. Kim, "Sol-gel synthesis and properties of multiferroic BiFeO_3 ", *Mater. Lett.*, **59** (2005) 4006–4009.
19. V. Fruth, M. Popa, D. Berger, R. Ramer, M. Gartner, A. Ciulei, M. Zaharescu, "Deposition and characterisation of bismuth oxide thin films", *J. Eur. Ceram. Soc.*, **25** (2005) 2171–2174.
20. V. Fruth, M. Popa, J. M. Calderón-Moreno, E.M. Anghel, D. Berger, M. Gartner, M. Anastasescu, P. Osiceanu, M. Zaharescu, "Chemical solution deposition and characterization of BiFeO_3 thin films", *J. Eur. Ceram. Soc.*, **27** (2007) 4417–4420.
21. A.H.M. Gonzales, A.Z. Simoes, L.S. Cavalcante, E. Longo, J.A. Varela, C.S. Ricardi, "Soft chemical deposition of BiFeO_3 multiferroic thin films", *Appl. Phys. Lett.*, **90** (2007) 052906.

22. A.Z. Simões, A.H.M. Gonzalez, L. S. Cavalcante, C. S. Riccardi, E. Longo, J.A. Varela, “Ferroelectric characteristics of BiFeO₃ thin films prepared via a simple chemical solution deposition”, *J. Appl. Phys.*, **101** (2007) 074108.
23. M.P. Pechini, “Method of preparing lead and alkaline earth titanates and niobates and coating method using the same to form a capacitor”, *U.S. Patent No.* 3330697, July 1967.
24. V. Fruth, D. Berger, C. Matei, A. Ianculescu, M. Popa, E. Tenea, M. Zaharescu, “Preparation and characterization of BiFeO₃ nanopowders”, *J. Phys. IV*, **128** (2005) 7–11.
25. M. Popa, D. Crespo, J. M. Calderon-Moreno, S. Preda, V. Fruth, “Synthesis and structural characterization of single-phase BiFeO₃ powders from a polymeric precursor”, *J. Am. Ceram. Soc.*, **90** (2007) 2723–2727.
26. M. Popa, S. Preda, V. Fruth, K. Sedlackova, C. Balazsi, D. Crespo, J.M. Calderon Moreno, “BiFeO₃ films on steel substrate by the citrate method”, *Thin Solid Films*, **517** (2009) 2581–2585.
27. M.K. Singh, M.H. Jang, S. Ryu, M.H. Jo, “Polarized Raman scattering of multiferroic BiFeO₃ epitaxial films with rhombohedral R3c symmetry” *Appl. Phys. Lett.*, **88** (2006) 042907, p.1–3.
28. R. Haumont, J. Kreisel, P. Bouvin, F. Hippert, “Phonon anomalies and the ferroelectric phase transition in BiFeO₃”, *Phys. Rev.*, **B73** (2006) 132101–132104.
29. D.A.G. Bruggeman, “Berechnung verschiedener physikalischer Konstanten von heterogenen Substanzen”, *Ann. Phys.*, **24** (1935) 636–679.
30. E. Palik, *Handbook of Optical Constants of Solids*, Academic Press Inc., NY, 1985.
31. V. Fruth, R. Ramer, M. Popa, J.M. Calderon-Moreno, E.M. Anghel, M. Gartner, M. Anastasescu, M. Zaharescu, “Deposition and characterization of BiFeO₃ thin films on different substrates”, *J. Mater. Sci.: Mater. Electron.*, **18** (2007) S187–S190.
32. T.L. Sudesh, L. Wijesinghe, J. Blackwood, “Electrochemical & optical characterization of passive films on stainless steels”, *J. Phys.: Conf. Series*, **28** (2006) 74–78.
33. Y.P. Wang, L. Zhou, M.F. Zhang, X.Y. Chen, J-M. Liu, Z-G. Liu, “Room-temperature structured ferroelectric polarisation in BiFeO₃ ceramics synthesized by rapid liquid phase sintering”, *Appl. Phys. Lett.*, **84** (2004) 1731–1733.
34. L. Mitoseriu, “Magnetoelectric phenomena in single-phase and composite systems”, *Bol. Soc. Esp. Ceram. V.*, **44** (2005) 77–84.
35. M. Mahesh Kumar, V.R. Palkar, K. Srivasan, S.C. Purndare, “Ferroelectricity in a pure BiFeO₃ ceramic” *Appl. Phys. Lett.*, **76** (2000) 2764–2766.
36. I. Sosnowska, T. Peterlin-Neumaier, E. Steichele, “Spiral magnetic ordering in bismuth ferrite”, *J. Phys. C: Solid State Phys.*, **15** (1982) 4835–4846.
37. G.D. Achenbach, W.J. James, R. Gerson, “Preparation of single-phase polycrystalline BiFeO₃”, *J. Am. Ceram. Soc.*, **50** [8] (1967) 437–437.
38. S. Shetty, V.R. Palkar, R. Pinto, “Size effect study in magnetoelectric BiFeO₃ system”, *Pramana J. Phys.*, **58** (2002) 1027–1030.
39. S. Ghosh, S. Dasgupta, A. Sen, H. S. Maiti, “Low-temperature synthesis of nanosized bismuth ferrite by soft chemical route”, *J. Am. Ceram. Soc.*, **88** (2005) 1349–1352.
40. V. Fruth, L. Mitoseriu, D. Berger, A. Ianculescu, C. Matei, S. Preda, M. Zaharescu, “Preparation and characterization of BiFeO₃ ceramic”, *Prog. Solid State Chem.*, **35** (2007) 193–202.
41. S. Chattopadhyay, S.D. Kelly, V.R. Palkar, L. Fan, C.U. Segre, “Investigation of size effects in magnetoelectric BiFeO₃”, *Phys. Scripta*, **T115** (2005) 709–713.
42. P. Royen, K. Swars, “Das System Wismutoxyd-Eisenoxyd Im Bereich Von 0 Bis 55 Mol-Percent Eisenoxyd”, *Angew. Chemie*, **69** (1957) 779–789.
43. M. Polomska, W. Kaczmarek, Z. Pajak, “Electric and magnetic-properties of (B_{1-x}La_x)FeO₃ solid-solutions”, *Phys. Status Solidi (A), Appl. Res.*, **23** (1974) 567–574.
44. S. Ghosh, S. Dasgupta, A. Sen, H.S. Maiti, “Low-temperature synthesis of nanosized bismuth ferrite by soft chemical route”, *J. Am. Ceram. Soc.*, **88** [5] (2005) 1349–1352.
45. J.D.G. Fernandes, D.M. A. Melo, L.B. Ziner, C.M. Salustiano, Z.R. Silva, A.E. Martinelli, M. Cerqueira, C. Alves Junior, E. Longo, M.I.B. Bernardi, “Low-temperature synthesis of single-phase crystalline LaNiO₃ perovskite via Pechini method”, *Mater. Lett.*, **53** (2002) 122–125.
46. Y. Ohno, S. Nagata, H. Sato, “Effect of electrode materials on the properties of high-temperature solid electrolyte fuel cells”, *Solid State Ionics*, **3-4** (1981) 439–442.
47. F.M. Figueiredo, J.R. Frade, F.M.B. Marques, “Electrical and electrochemical behavior of LaSrCoO_{3±δ}+La₂(Zr,Y)₂O₇-based electrode materials”, *Solid State Ionics*, **118** (1999) 81–87.
48. Y. Teraoka, H.M. Zhang, K. Okamoto, N. Yamazoe, “Mixed ionic-electronic conductivity of La_{1-x}Sr_xCo_{1-y}Fe_yO_{3-δ} perovskite-type oxides”, *Mater. Res. Bull.*, **23** (1988) 51–58.
49. F.M. Figueiredo, F.M.B. Marques, J.R. Frade, “Electrochemical permeability measurements of La_{1-x}Sr_xCoO_{3±δ} materials”, *Solid State Ionics*, **111** (1998) 273–281.
50. H.J. Hwang, J. Moon, M. Awano, K. Maeda, “Sol-gel route to porous lanthanum cobaltite (LaCoO₃) thin films”, *J. Am. Ceram. Soc.*, **83** (2000) 2852–2854.
51. K. Kleveland, N. Orlovskaya, T. Grande, A.M. Mardal Moe, M.-A. Einarsrud, K. Breder, G. Gogotsi, “Ferroelastic behavior of LaCoO₃-based ceramics”, *J. Am. Ceram. Soc.*, **84** (2001) 2029–2033.

52. N. Orlovskaya, K. Kleveland, T. Grande, M.-A. Einarssrud, “Ferroelasticity in mixed conducting LaCoO_3 based perovskites: A ferroelastic phase transition”, *J. Eur. Ceram. Soc.*, **20** (2000) 51–56.
53. R.A. De Souza, J.A. Kilner, “Oxygen transport in $\text{La}_{1-x}\text{Sr}_x\text{Mn}_{1-y}\text{Co}_y\text{O}_{3\pm d}$ perovskites: Part I. Oxygen tracer diffusion”, *Solid State Ionics*, **106** [3-4] (1998) 175–187.
54. S.T. Aruna, M. Muthuraman, K.C. Patil, “Studies on combustion synthesised LaMnO_3 - LaCoO_3 solid solutions”, *Mater. Res. Bull.*, **35** (2000) 289–296.
55. M. Popa, J.M. Calderon-Moreno, “Lanthanum cobaltite thin films on stainless steel”, *Thin Solid Films*, **517** (2009) 1530–1533.
56. M. Popa, J.M. Calderon-Moreno, “Lanthanum cobaltite nanoparticles using the polymeric precursor method”, *J. Eur. Ceram. Soc.*, **29** (2009) 2281–2287.
57. D. Berger, C. Matei, F. Papa, G. Voicu, V. Fruth, “Pure and doped lanthanum cobaltites obtained by combustion method”, *Progr. Solid State Ch.*, **35** (2007) 183–191.
58. T. Yao, Y. Uchimoto, T. Sugiyama, Y. Nagai, “Synthesis of $(\text{La,Sr})\text{MeO}_3$ (Me = Cr, Mn, Fe, Co) solid solution from aqueous solutions”, *Solid State Ionics*, **135** (2000) 359–364.
59. E. Bontempi, L. Armelao, D. Barreca, L. Bertolo, G. Bottaro, E. Pierangelo, L.E. Depero, “Structural characterization of sol-gel lanthanum cobaltite thin films”, *Crystal Eng.*, **5** (2002) 291–298.
60. S. Nakayama, M. Okazaki, Y.L. Aung, M. Sakamoto, “Preparations of perovskite-type oxides LaCoO_3 from three different methods and their evolution by homogeneity, sinterability and conductivity”, *Solid State Ionics*, **158** (2003) 133–139.
61. S. Faaland, T. Grande, M.-A. Einarssrud, P.E. Vullum, R. Holmestad, “Stress-strain behavior during compression of polycrystalline $\text{La}_{1-x}\text{Ca}_x\text{CoO}_3$ ceramics”, *J. Am. Ceram. Soc.*, **88** (2005) 726–730.
62. D. Berger, N. van Landschoot, C. Ionica, F. Papa, V. Fruth, “Synthesis of pure and doped lanthanum cobaltite by the combustion method”, *J. Optoelectron. Adv. Mater.*, **5** (2003) 719–724.
63. F. Li, X. Yu, L. Chen, H. Pan, X. Xin, “Solid-state synthesis of LaCoO_3 perovskite nanocrystals”, *J. Am. Ceram. Soc.*, **85** (2002) 2177–2180.
64. M. Popa, J. Frantti, M. Kakihana, “Characterization of LaMeO_3 (Me: Mn, Co, Fe) perovskite powders obtained by polymerizable complex method”, *Solid State Ionics*, **154-155** (2002) 135–141.
65. J. Guo, H. Lou, Y. Zhu, X. Zheng, “La-based perovskite precursors preparation and its catalytic activity for CO_2 reforming of CH_4 ”, *Mater. Lett.*, **57** (2003) 4450–4455.
66. H. Taguchi, S. Yamada, M. Nagao, Y. Ichikawa, K. Tabata, “Surface characterization of LaCoO_3 synthesized using citric acid”, *Mater. Res. Bull.*, **37** (2002) 69–76.
67. S. Ajami, Y. Mortazavi, A. Khodadadi, F. Pourfayaz, S. Mohajezadeh, “Highly selective sensor to CH_4 in presence of CO and ethanol using LaCoO_3 perovskite filter with Pt/SnO_2 ”, *Sensors Actuat. B*, **117** (2006) 420–425.
68. L. Predoana, A. Jitianu, B. Malic, M. Zaharescu, “Study of the gelling process in the La-Co-citric acid system”, *J. Sol-Gel Sci. Technol.*, submitted.
69. L. Predoana, B. Malic, M. Kosec, M. Carata, M. Caldararu, M. Zaharescu, “Characterization of LaCoO_3 powders obtained by water-based sol-gel method with citric acid”, *J. Eur. Ceram. Soc.*, **27** (2007) 4407–4411.
70. L. Predoana, B. Malic, M. Kosec, M. Scurtu, M. Caldararu, M. Zaharescu, “Phase formation and electrical properties of the LaCoO_3 obtained by water-based sol-gel method with citric acid”, *Process. Applic. Ceram.*, **3** (2009) 39–42.
71. L. Predoana, B. Malic, M. Zaharescu, “ LaCoO_3 formation from precursors obtained by water-based sol-gel method with citric acid”, *J. Therm. Anal. Cal.*, **98** (2009) 361–366.
72. A.B.P. Lever, *Inorganic Electronic Spectroscopy*, Second Edition, Elsevier, New York, 1984.
73. K. Nakamoto, *Infrared and Raman Spectra of Inorganic and Coordination Compounds Part B., Applications in Coordination, Organometallic and Bioinorganic Chemistry*, Sixth Edition, John Wiley & Sons Inc., New-York, 2009.
74. R. Schmidt, J. Wu, C. Leighton, I. Terry, “Dielectric response to the low-temperature magnetic defect structure and spin state transition in polycrystalline LaCoO_3 ”, *Phys.Rev.B.*, **79** (2009) 125105-1-8.
75. L. Predoana, B. Malic, D. Crisan, N. Dragan, M. Gartner, M. Anastasescu, J. Calderon-Moreno, M. Zaharescu, “Sintering behavior of LaCoO_3 powders obtained by aqueous sol-gel method starting with different precursors”, pp. 22–24 in *Proceedings of 11th Conference of the European Ceramics Society, CD-ROM, Session A*, Krakow, Poland, 2009.